frontiers | Frontiers in Energy Research

TYPE Original Research
PUBLISHED 29 December 2023
DOI 10.3389/fenrg.2023.1338391

OPEN ACCESS

EDITED BY
Qiang Liu,
China University of Petroleum, China

REVIEWED BY
Yongqiang Feng,
Jiangsu University, China
Fubin Yang,
Beijing University of Technology, China

*CORRESPONDENCE
Xurong Wang,
xurong.wang@huuc.edu.cn

RECEIVED 14 November 2023
ACCEPTED 08 December 2023
PUBLISHED 29 December 2023

CITATION
Jiang X, Zhang X, Wang R and Wang X (2023), Comparative study of thermally integrated pumped thermal energy storage based on the organic rankine cycle with different working fluid pairs. *Front. Energy Res.* 11:1338391. doi: 10.3389/fenrg.2023.1338391

Comparative study of thermally integrated pumped thermal energy storage based on the organic rankine cycle with different working fluid pairs

Xuhui Jiang[1], Xi Zhang[1], Ruiqiong Wang[1] and Xurong Wang[2]*

[1]PowerChina Chongqing Engineering Co., Ltd., Chongqing, China, [2]School of Energy and Building Environment Engineering, Henan University of Urban Construction, Pingdingshan, China

Thermal integrated pumped thermal energy storage (TIPTES) systems with the features of high efficiency, flexibility, and reliability, have attracted increasing attention since they can integrate low-grade heat sources to further improve the utilization and economic viability of renewable energy. In this study, a typical TIPTES system driven by waste flue gas is established, and the heat pump and organic Rankine cycle (ORC) are chosen as the charging and discharging cycle, respectively. Four organic fluids, including R600, R245fa, R601a, and R1336mzz(Z), are selected to compose sixteen different working fluid pairs for thermodynamic analysis. The effects of key parameters, like heat pump system evaporation temperature and hot storage tank temperature, on system performance were analyzed, and the single-objective optimization was conducted. A comparative study was carried out to identify the best working fluid pair according to the optimization results. Results show that the system's power-to-power efficiency goes up as the evaporation temperature increases while an increase in the heat storage temperature decreases the exergy efficiency of the TIPTES system. Optimization results show that the R245fa + R245fa is the best working fluid pair, and in this system, the ORC evaporator has the largest exergy destruction at about 260.84 kW, which is 20.2% of the total. On the other hand, the ORC pump has the smallest exergy destruction only about 0.5%. This study also finds that the system's power-to-power efficiency of using different working fluids in either heat pump cycles or ORC cycles is lower than that of using the same working fluid throughout the entire system.

KEYWORDS

organic rankine cycle, thermally integrated, pumped thermal energy storage, thermodynamic analysis, comparative study

1 Introduction

With the rapid development of economic society and technology, massive emissions of greenhouse gases such as carbon dioxide and methane caused by human activities have become the main cause of global climate change (Liu Z. et al., 2023). To achieve the goal of carbon neutrality, many countries propose to vigorously develop renewable energy sources represented by solar energy, wind energy, and so on (Li et al., 2021). This move can effectively improve the current situation of relying on fossil energy for energy supply and mitigate environmental problems taken from the energy supply processes (Wang S. et al.,

2023; Lin and Zhang, 2023). According to a survey by the International Energy Agency, the scale of renewable energy will expand rapidly over the next few years, and be the largest source of electricity supply by early 2025 (Agency and International Energy, 2022). Since typical renewable energies, like solar and wind, have features of instability and intermittency, it brings a great challenge for its integration into the power system (Fu et al., 2021). Therefore, energy storage systems are seen as an effective way to address this challenge and an important part of the energy mix transition at this stage (Zhang et al., 2023).

Energy storage technologies contain mechanical energy storage, thermal energy storage, electrochemical energy storage, chemical energy storage, etc. (Olabi et al., 2021). Among them, pumped hydro energy storage is mainly limited by geographic location and low energy density (Amirante et al., 2017). Flywheel energy storage technology has higher power and energy density, but also higher relative costs and losses (Olabi et al., 2021). Electrochemical energy storage technologies have the advantages of high energy density and flexibility and can be integrated into electrical systems, but they are costly and may be harmful to the environment (Luo et al., 2015; Deguenon et al., 2023). Chemical energy storage, including hydrogen storage and fuel cells, fits well with net-zero emission standards, but its high cost and risk cannot be ignored (Olabi et al., 2021; Deguenon et al., 2023). Moreover, as energy storage technology continues to evolve, pumped thermal energy storage (PTES) has attracted much attention due to its small investment cost, high round-trip efficiency, long service life, and lack of geographical constraints, when compared to pumped hydro energy storage and compressed air energy storage (Benato and Stoppato, 2018; Frate et al., 2021).

PTES is a new energy storage technology that can convert electrical energy into heat and store it in a high-temperature heat storage device, and release the energy when it is needed (Zhang and Xie, 2022). Blanquiceth et al. (2023) evaluated the effectiveness of PTES systems integrated with large-scale thermal power plants and concluded that the RTE can be more than 50% and that it can be greater than 63% in modern supercritical Rankine cycles. Tafone et al. (2023) developed a composite dynamic numerical model to evaluate a proposed CHEST structure based on cascades of PMC-based energy storage, with significant improvement in round-trip efficiency. Zhao et al. (2023) conducted multi-objective economic optimization of PTES systems with a power capacity of 10 MW and a discharge time of 6 h and concluded that magnetite as a solid storage material and helium as a working fluid are the optimal choices for systems with STR.

In contrast to the PTES systems that rely on the trans-critical CO_2 cycle and the Brayton cycle, the PTES utilizing the organic Rankine cycle (ORC) as the discharge cycle demonstrates superiority when low-grade heat sources are utilized for energy storage (Wang et al., 2021; Wang P. et al., 2022; Wang S. et al., 2022; Tang et al., 2022; Liu L. et al., 2023; Wang P. et al., 2023; Tang et al., 2023). Tillmanns et al. (2022) investigated the thermo-economic potential of PTES systems based on the ORC, and C3 and alkenes are more promising as working fluids for the ORC through computational molecular-assisted design methods. Eppinger et al. (2020) investigated the effect of several different fluids, and R1233zd(E) was probably the best choice after taking into account efficiency and environmental and safety considerations, and cyclopentane achieved the highest efficiency for latent storage. Peterson (2011) analyzed the model for storing electrical power by latent heat using PTES. They investigated the working process of the expander/compressor under small temperature differentials, predicting power-to-power efficiencies in the range of 50%–60% when utilizing ordinary refrigerants.

Compared to ordinary ORC-PTES, the thermally integrated PTES (TIPTES) can make better use of low-grade thermal energy and obtain higher thermal efficiency (Frate et al., 2017; Ökten and Kurşun, 2022). Wang P. et al. (2022) investigated the effect of five different working fluids on the thermodynamic and thermo-economic performances of different systems and found that the best choices for ORC-TIPTES and OFC-TIPTES were cyclohexane and butane, respectively. Ökten and Kurşun (2022) integrated an absorption refrigeration cycle (ARC) into the TIPTES system. A thermodynamic analysis of the system revealed a performance improvement ranging from 15.3% to 41.5%. Hu et al. (2021) evaluated the thermal economy of the TI-PTES system with different typical heat source scenarios and found that an increased heat supply rate/temperature results in improved component efficiency, and that a reduced temperature difference at the pinch point leads to increased efficiency or decreased expenses. Jockenhöfer et al. (2018) proposed a PTES system based on subcritical total heat integration using butene as the working fluid, and it was found that the maximum round-trip efficiency was 1.25 at a heat source temperature of 100°C and a heat sink temperature of 15°C, while 0.59 was the maximum exergy efficiency.

Based on the above studies, the current research on TIPTES mainly focuses on the charging cycle and discharging cycle with the same working fluid, but the research on the charging and discharging cycle with different working fluids is relatively insufficient. Fan and Xi (2022a) established a Carnot cell model with two different working fluid pairs and showed that the system has the best economy when the R1336mzz(Z)+R245fa working fluid pair is employed in the HP and ORC, respectively, and the system has the highest exergy efficiency when the R245fa + HFO-1336mzz(Z) working fluid pair is used. However, they only used two types of working fluids in the study. Xue et al. (2022) proposed a PTES system integrated with waste heat, simultaneously screening 22 organic working fluids. Ultimately, the optimal working fluid suitable for the system was selected, and a performance analysis, as well as multi-objective optimization, were conducted. However, this paper exclusively investigates scenarios where the charging and discharging cycles use the same working fluid, neglecting situations where the two cycles use different working fluids.

In the current study, most researchers typically use the same fluid as the working fluid for charge and discharge cycles (Wang et al., 2020; Wang S. et al., 2022; Yu et al., 2023). In addition, the researchers found that mixing several pure working fluids to form a hybrid working fluid with complementary advantages. In particular, utilizing the temperature slip characteristics of the phase transition process of non-eutectic working fluid can effectively reduce the irreversible losses in the heat transfer process and improve the efficiency of the thermal cycle (Sun et al., 2019; Wang et al., 2019; Blondel et al., 2023). However, in current research on the TIPTES system using different working fluids, there is a limitation in the variety of employed fluids or a tendency to use the same working

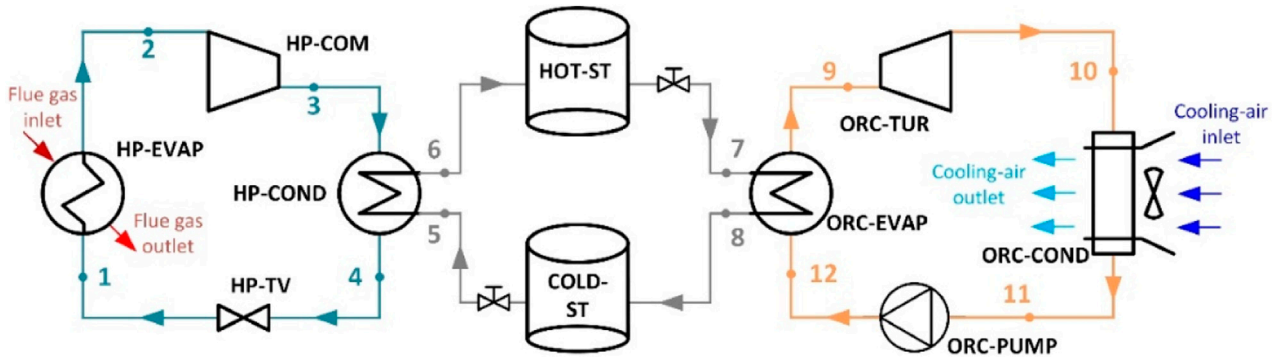

FIGURE 1
Schematic diagram of a typical TIPTES system.

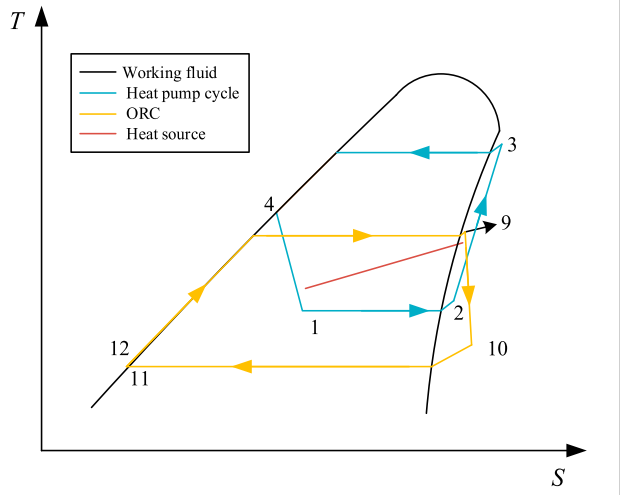

FIGURE 2
T-s diagram of a typical TIPTES system.

fluid in both the charging and discharging cycles. The impact of different fluid combinations on system performance needs further investigation. In this paper, four different working fluids of R600, R245fa, R601a, and R1336mzz(Z) are combined in pairs and applied to the charging and discharging cycles respectively, and the system performance and economy are specifically analyzed through numerical simulation and single-objective optimization. The contributions of this article are as follows:

1) The system involves a selection and pairing of four distinct working fluids to optimize charging and discharging cycles.
2) The system employs a single-objective optimization method to establish the most conducive design parameters.

In this paper, Section 2 constructs an ORC-TIPTES system and picks the working fluids. In Section 3, the article presents the mathematical models of energy and exergy functions for the system accordingly. Section 4 introduces genetic algorithms and describes the implementation of single-objective optimization. The fifth section displays the model verification of the ORC-TIPTES system. Section 6 then analyses and discusses the parametric analysis of the system and the results of the single-objective optimization.

2 System construction and fluid selection principle

The waste flue gas was taken as a low-temperature heat source for the ORC-TIPTES. Figure 1 and Figure 2 respectively show the system form of the ORC-TIPTES and the related T-s diagram. The ORC-TIPTES consists of a heat source (flue gas), an HP subsystem, an ORC subsystem, and a thermal energy storage subsystem (TES), which includes two evaporators, two condensers, a compressor, throttle valves, a turbine, a pump, and two storage tank. Water was chosen as the energy storage medium in this system due to its high heat capacity, stability, availability, and low cost.

The working process of the ORC-TIPTES mainly contains charging, discharging, and energy storage processes. For the charging process of the system, the working fluid at low temperature and low pressure absorbs waste heat from the flue gas through the heat pump evaporator and is vaporized into superheated steam (1–2). Then, the working fluid is compressed by the compressor driven by excess electricity from the grid (2–3). Afterward, the high-temperature and high-pressure working fluid releases heat through the heat pump condenser to transfer heat to the thermal storage medium, which is stored in the thermal storage tank (three to four and 5–6). The condensed medium is throttled through a throttle valve to become a low-temperature and low-pressure liquid and then reenters the evaporator (4–1) to complete the cycle. During the discharging process of the system, the refrigerant absorbs heat in the thermal storage tank through the ORC evaporator, which becomes superheated steam (12–9). As the high-temperature and high-pressure working fluid enters the turbine, it expands and converts its thermal energy into mechanical energy (9–10). Subsequently, the turbine generates electricity by utilizing the low-pressure steam produced during the expansion process. Then, the exhaust gas from the turbine is cooled by air in the ORC condenser (10–11), and the saturated liquid flowing out of the condenser is pressurized by a pump (11–12) which reenters the evaporator to complete the process again.

TABLE 1 Input parameters of the TIPTES system.

Parameter	Symbol	Value	Unit
Ambient pressure	P_0	101.325	kPa
Ambient temperature	T_0	20	℃
Heat source temperature	T_{hs}	90	℃
Thermal storage temperature	T_{hs}	100–135	℃
Mass flow rate of heat source	m_{hs}	55	kg/s
Pinch point of heat exchanger	T_{pp}	5	℃
Superheat degree of evaporator	T_s	8	℃
Compressor efficiency	η_{com}	0.80	-
Pump efficiency	η_{pum}	0.75	-
Turbine efficiency	η_{tur}	0.85	-
Storage duration	τ	6	h

The basic input parameters of the ORC-TIPTES system are displayed in Table 1. To make the calculation easier, the simplifying assumptions were made as follows:

1) The system operated in a stable state.
2) Pressure drops during the flow were neglected.
3) Heat losses during the flow were ignored.
4) The efficiencies of the components were constant.

The choice of the working fluid as the energy carrier in a thermodynamic cycle plays a decisive role in the performance of the system (Liang et al., 2022). An appropriate working fluid can maximize the efficiency of the system and improve its economy and reliability. When selecting a working fluid, it is necessary to consider not only its physical and chemical properties but also its environmental friendliness, safety, price, and other aspects. Currently, there is no perfect working fluid candidate that is suitable for all operating conditions. Therefore, considering the thermophysical properties and environmental friendliness of the working fluid, the main parameters of the four selected working fluids are listed in Table 2, which include R600, R245fa, R601a, and R1336mzz(Z). They are all dry fluids, which could improve the performance of the system, also reduce the system investment and operating costs (Bao and Zhao, 2013). For this research, the ozone depletion potential of the R600 and R601a is 0, and the global warming potential is very low, which is environmental friendliness. However, the R245fa and R1336mzz(Z) with zero ODP but relatively higher GWP are also acceptable due to their wide range of engineering applications (Wang Q. et al., 2022).

3 Mathematical models

For the heat exchangers of the system, the thermal transfer can be calculated as:

$$Q_{he} = m_w (h_{out} - h_{in}) \tag{1}$$

where Q_{he} is the heat transfer amount of the heat exchangers evaporator and condenser; m_w is the mass flow rate of the fluid; and h is the specific enthalpy. The subscripts of 'in' and 'out', respectively, indicate heat exchanger import and export.

The consumed power of the compressor can be expressed as:

$$W_{com} = m_w (h_{com,out} - h_{com,in}) = m_w (h_{com,out(a)} - h_{com,in})/\eta_{com} \tag{2}$$

The power consumption of the pump and the output power of the turbine can be expressed as:

$$W_{pum} = m_w\left(h_{pum,out} - h_{pum,in}\right) = m_w\left(h_{pum,out(a)} - h_{pum,in}\right)/\eta_{pum} \tag{3}$$

$$W_{tur} = m_w (h_{tur,out} - h_{tur,in}) = m_w (h_{tur,out(a)} - h_{tur,in})/\eta_{tur} \tag{4}$$

where $h_{out(a)}$ is the isentropic enthalpy; η_{com}, η_{pum}, and η_{tur} are respectively the isentropic efficiency of the compressor, pump, and turbine which are defined as follows:

$$\eta_{com} = (h_{com,out(a)} - h_{com,in})/(h_{com,out} - h_{com,in}) \tag{5}$$

$$\eta_{pum} = (h_{pum,out(a)} - h_{pum,in})/(h_{pum,out} - h_{pum,in}) \tag{6}$$

$$\eta_{tur} = (h_{tur,out(a)} - h_{tur,in})/(h_{tur,out} - h_{tur,in}) \tag{7}$$

The net power output W_{np} of the system is:

$$W_{np} = W_{tur} - W_{pum} \tag{8}$$

In the entire system, the energy balance equation can be expressed as.

$$\Sigma m_{in} h_{in} + Q = \Sigma m_{out} h_{out} + W \tag{9}$$

where h represents the specific enthalpy; m represents the mass flow rate; W represents the output power of the system and Q represents the heat absorption amount.

In the research, power-to-power efficiency is an important indicator to evaluate the performance of PTES systems, which is defined as:

TABLE 2 Basic thermo-physical properties of different organic fluids.

Working fluid	Physical data			Environmental data	
	Molecular mass/g·mol^{-1}	T_{crit}/K	p_{crit}/MPa	GWP 100 years	ODP
R600	58.12	425.13	3.796	20	0
R245fa	134.05	427.16	3.651	1030	0
R601a	72.15	460.35	3.378	20	0
R1336mzz(Z)	164.06	444.50	2.903	1280	0

$$\eta_{ptp} = \eta_{ts}\eta_{dt}COP \tag{10}$$

where η_{ts} refers to the TES system efficiency, η_{dt} refers to the discharging thermal efficiency which is set to be 1 (Eppinger et al., 2021), and *COP* refers to the HP cycle coefficient of performance which is defined as follows:

$$COP = \frac{Q_{ts}}{W_{com}} \tag{11}$$

where Q_{ts} expresses the storage tank's heat storage amount. The discharging part's thermal efficiency can be defined as:

$$\eta_{dt} = \frac{W_{np}}{Q_{ts}} \tag{12}$$

Generally, the temperature sequence of each part in the system is as follows:

$$T_{ts} > T_{hs} > T_0 \tag{13}$$

Based on the concept of the Carnot cycle, the maximum *COP* of the HP and η_{dt} at the same temperature condition can be calculated as:

$$COP_{max} = \frac{T_{ts}}{T_{ts} - T_{hs}} \tag{14}$$

$$\eta_{dt,max} = \frac{T_{ts} - T_0}{T_{ts}} \tag{15}$$

Therefore, $\eta_{ptp,\ max}$ can be obtained from the above formulas as follows:

$$\eta_{ptp,max} = \frac{T_{ts}}{T_{ts} - T_{hs}} \cdot \frac{T_{ts} - T_0}{T_{ts}} = 1 + \frac{T_{hs} - T_0}{T_{ts} - T_{hs}} > 1 \tag{16}$$

where the maximum η_{ptp} of the TIPTES system may exceed 100% if adding low-grade heat sources (Bellos et al., 2021).

For exergy analysis, the physical exergy of each stream in the whole system be calculated as:

$$E = m[(h - h_0) - T_0(s - s_0)] \tag{17}$$

where s_0 refers to the specific entropy and h_0 refers to the specific enthalpy in T_0.

The components' exergy destruction of the system is as follows.

$$\Sigma E_d = \Sigma E_{in} - \Sigma E_{out} \tag{18}$$

The exergy efficiency η_{ex} of the system is as follows:

$$\eta_{ex} = \frac{E_{dt}}{E_{hs} + E_{HP}} = \frac{E_{HP}\eta_{PTP}}{E_{hs} + E_{HP}} \tag{19}$$

$$E_{HP} = \frac{Q_{hs}}{COP - 1}\tau \tag{20}$$

$$E_{hs} = m_{hs}\tau\left[\left(h_{hs,max} - h_{hs,min}\right) - T_0\left(s_{hs,max} - s_{hs,min}\right)\right] \tag{21}$$

where E_{hs} refers to the additional heat source exergy, E_{hp} refers to the electric energy exergy, s_{hs} refers to additional heat source entropy, h_{hs} refers to the additional heat source enthalpy, and τ denotes thermal energy storage duration.

4 Single-objective optimization method

To solve the single-objective optimization problem of ORC-TIPTES, a genetic algorithm (GA) is chosen in this study. The GA generates a variety of new populations through the selection, crossover, and mutation of a series of individuals in the current population, and gradually makes the population evolve to the desired optimal state. Because of its adaptability and parallel processing ability, genetic algorithm has been widely used in many fields, such as engineering optimization, machine learning, scheduling problems, and so on.

System performance evaluation needs to consider the different parameters affecting thermodynamic performance simultaneously. In this paper, system power efficiency and exergy efficiency are selected as optimization objective functions. For the ORC-TIPTES, $T_{eva,\ hp}$, T_{cs}, and T_{ts} are the main parameters of system performance taken for the decision variables. In this study, $T_{eva,\ hp}$ refers to the HP system evaporation temperature, T_{cs} refers to the cold storage tank temperature, and T_{ts} refers to the hot storage tank temperature. Table 3 shows the range of the various decision variables, and the optimization results of the system are shown in Table 4. The population size set in the genetic algorithm is 50, the generation set is 15, and the Pareto fraction is 0.9.

5 Model validation

Model verification is a key step to verify the accuracy of research. Therefore, the feasibility of the HP system and ORC system is verified by comparing them with the research data in the literature (Hu et al., 2021; Fan and Xi, 2022b). The results of specific data comparisons between this paper and the literature are listed in Table 3 and Table 4. It is found that the error between the results in this paper and those in the literature is very small by the model verification results. Therefore, the model is feasible in this paper.

6 Results and discussions

Based on the physical model and mathematical model of the ORC-TIPTES established above, the influence of different working fluid pairs on the key parameters T_1 and T_6 on the system performance should be analyzed. Meanwhile, in this paper, the term "working fluid pairs" refers to the use of the same or different pure working fluids in the charging and discharging cycles. The way (working fluid 1 + working fluid 2) is adopted to express the working fluid pair, and the former represents the fluid in the HP subsystem during the charging process while the latter denotes the fluid in the ORC subsystem during the discharging process.

6.1 Parameter analysis

Figure 3 shows the changing trend of η_{ptp} as T_6 increases. As T_6 increases, the η_{ptp} of all groups shows a significant downward trend. When R600 and R245fa are used as working media in the heat pump cycle, the eight efficiency curves overlap almost completely throughout the entire stage of increasing storage temperature. Before reaching 115°C, the η_{ptp} of all groups are not significantly different, but gradually begin to show larger differences after the temperature rises to 120°C. Among all working fluid groups, the

TABLE 3 Model validation of the HP subsystem.

Basic parameters		Data from the literature Fan and Xi (2022b)	This work
Input values	Isentropic efficiency of the compressor	0.80	0.80
	Pinch point temperature difference	5°C	5°C
	Superheat degree in evaporator	2°C	2°C
Output values	$\dot{Q}_{eva}$	3963 kW	3966 kW
	$\dot{W}_{comp}$	1392 kW	1393 kW
	$\dot{Q}_{con}$	5355 kW	5362 kW

TABLE 4 Model validation of the ORC subsystem.

States	*P*/(kPa)			*T*/(°C)			*h*/(kJ/kg)		
	This study	Ref. Hu et al. (2021)	Error (%)	This study	Ref. Hu et al. (2021)	Error (%)	This study	Ref. Hu et al. (2021)	Error (%)
1	624	624	0.00	90	90	0.00	434.43	434.43	0.00
2	110.21	110	0.19	43.92	44.32	−0.90	409.55	409.70	−0.04
3	109.72	110	−0.25	30.32	30	1.07	230.34	230.26	0.03
4	623.65	624	−0.06	30.53	30.27	0.86	229.58	230.70	−0.49
5	101.23	101	0.23	24.86	25	−0.56	105.22	104.92	0.29
6	100.83	101	−0.17	27.55	27.12	1.59	114.21	113.78	0.38

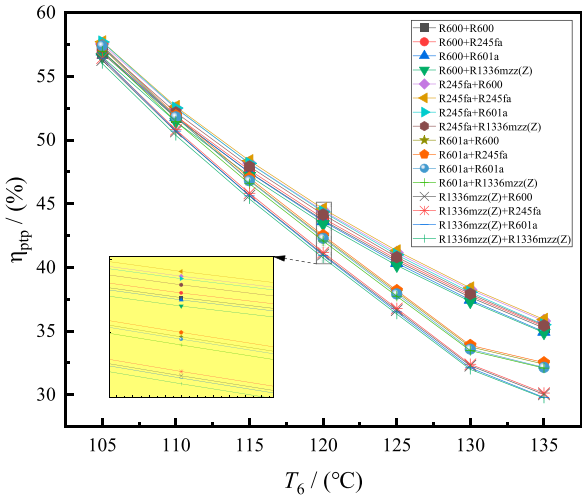

FIGURE 3
Effects of T_6 on the η_{ptp}.

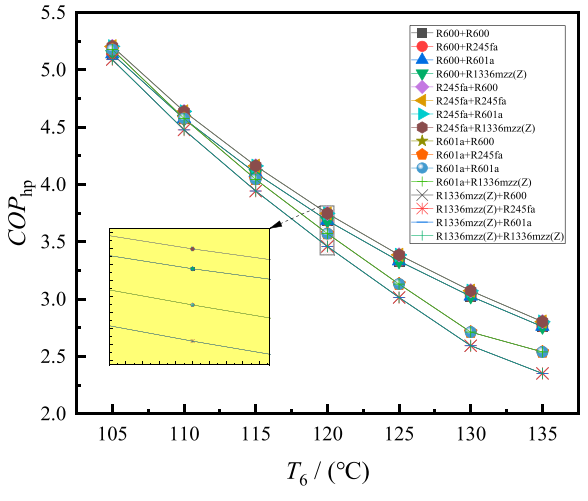

FIGURE 4
Effects of T_6 on the η_{ORC}.

system corresponding to R245fa + R245fa exhibits the highest η_{ptp} when T_6 decreases. When the heat storage temperature is 105°C, it reaches its optimal value of 63.59% and its minimum value of 35.91% occurs at a heat storage temperature of 135°C.

Figure 4 and Figure 5 show the changing trends of η_{ORC} and COP_{hp} along with the change of T_6, respectively. It can be seen from Figure 4 that η_{ORC} generally shows a linear upward trend when T_6 rises from 105°C to 135°C. However, COP_{hp} showed the same downward trend as η_{ptp} in Figure 5, and the overlap of the curves is also highly similar to Figure 3. According to Eq. 11, COP_{hp} is determined by the ratio between the heat stored in the thermal energy storage system and the work done by the

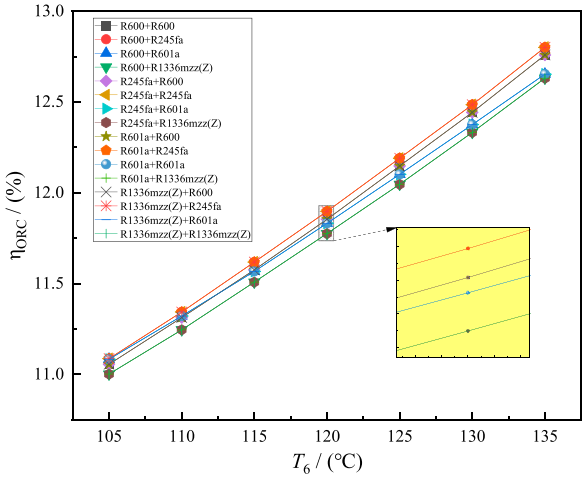

FIGURE 5
Effects of T_6 on the COP_{hp}.

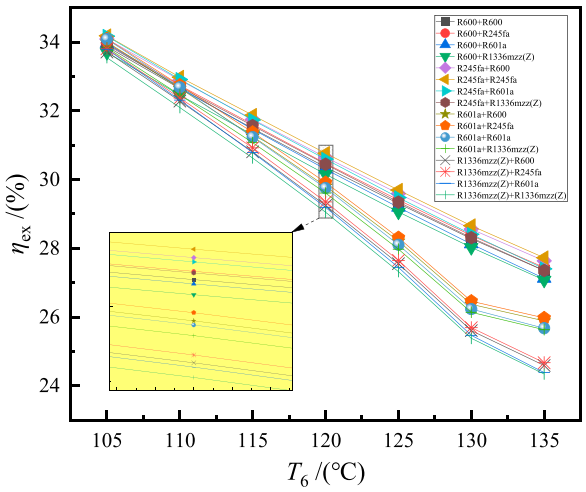

FIGURE 6
Effects of T_6 on the η_{ex}.

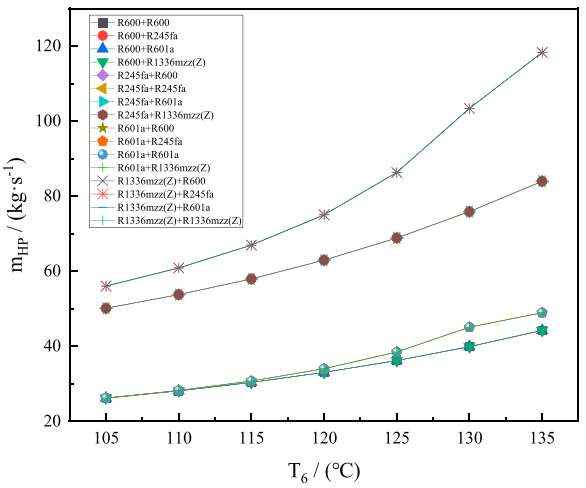

FIGURE 7
Effects of T_6 on the m_{hp}.

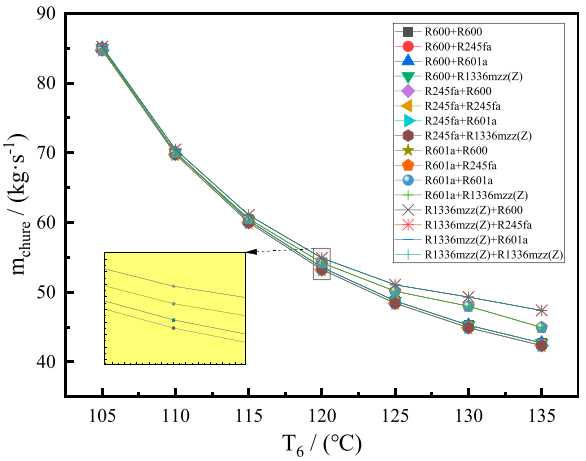

FIGURE 8
Effects of T_6 on the m_{churre}.

compressor. As T_6 increases, the difference in enthalpy values between state points 3 and 4 in Figure 1 decreases, resulting in a smaller increase in stored heat compared to the increased work done by the compressor. This phenomenon leads to a reduction in COP_{hp}.

In the case of the R245fa + R245fa working fluid pair, its η_{ORC} also increases from the lowest point of 11.09% to the highest point of 12.8% as T_6 rises. Concurrently, the COP_{hp} sharply decreases from its peak of 5.87 to 2.8, representing a reduction of over 50%. The above results indicate that the impact of COP_{hp} on η_{ptp} is greater than the effect of η_{ORC}, and it is the primary factor causing the change in efficiency.

The η_{ex} is also an important indicator for evaluating the effectiveness of energy conversion and utilization. Figure 6 indicates the effects of T_6 on the η_{ex}. It is shown that the diagram is roughly divided into four sections because of the use of four different working fluids in the heat pump cycle, but the general trend is a linear decrease. The working fluid pair of R245fa + R245fa exhibits optimal characteristics, in which its maximum value at 105°C is 34.18%, and the minimum value at 135°C is 27.72%.

Assuming constant closed loop flow rates in the HP cycle, storage loop, and ORC during system operation, variations in m_{hp}, m_{churre}, and m_{ORC} are shown in Figure 7, Figure 8, Figure 9, respectively. It can be seen that m_{hp} and m_{ORC} decrease with the increase of T_6, but m_{churre} increases. For m_{hp}, due to the different working fluids in the HP subsystem, the 16 working fluid pairs finally show four general trends. R1336mzz(Z) has the highest maximum m_{hp} when used as the working fluid in the HP subsystem, while R600 and R601a have relatively smaller values. In Figure 8, overall differences among all working fluid pairs are small, especially before warming up to 115°C, where the 16 curves almost overlap.

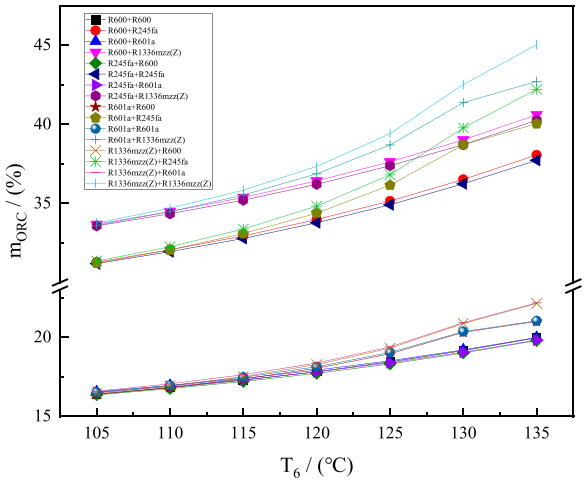

FIGURE 9
Effects of T_6 on the m_{ORC}.

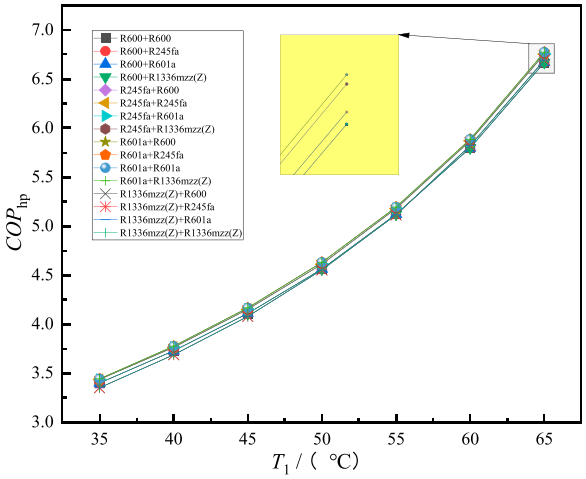

FIGURE 11
Effects of T_1 on the COP_{hp}.

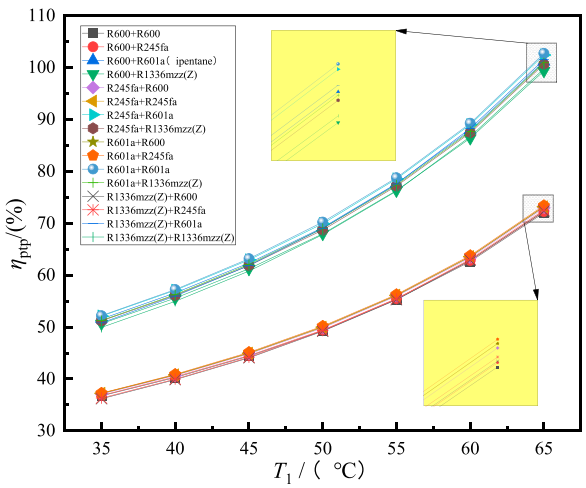

FIGURE 10
Effects of T_1 on the η_{ptp}.

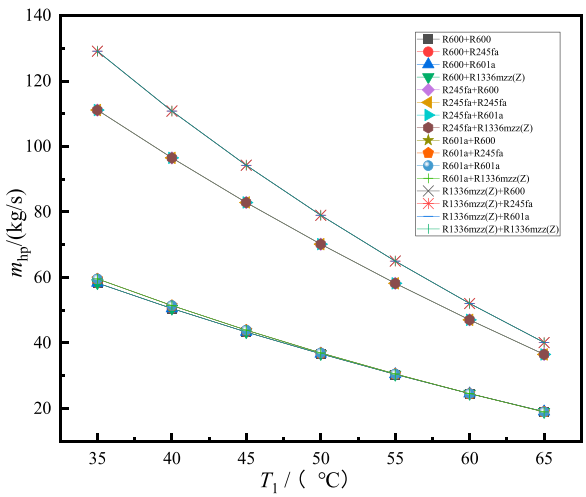

FIGURE 12
Effects of T_1 on the m_{hp}.

T_1 is also an important parameter affecting the performance of the system. For 16 working fluid pairs, the effects of T_1 on η_{ptp} of ORC-TIPTES are depicted in Figure 10. According to Figure 10, the trends of η_{ptp} are similar. Generally, when T_1 increases, the values of η_{ptp} increases. The maximum value of η_{ptp} is 102.74% in the working fluid pair of R601a + R601a at T_1 of about 65°C, and the minimum value of η_{ptp} is 72.04% in the working fluid pair of R600 + R600. Therefore, since the working fluid pair of R601a + R601a demonstrates good thermodynamic performance, it is selected as one of the objects for single-objective optimization analysis.

The effects of T_1 on COP_{hp} are shown in Figure 11. In the T_1 range of 35–65°C, COP_{hp} of working fluid pair R601a + R601a is maximal, and COP_{hp} of working fluid pair R600 + R600 is minimum. The trend observed in these results is largely consistent with the effects of T_1 on η_{ptp}, indicating that COP_{hp} values play a dominant role in the variation of η_{ptp} with T_1. This also further confirms the superior thermodynamic performance of the working fluid pair R601a + R601a.

Figure 12 shows the effects of T_1 on m_{hp}. The m_{hp} generally exhibits a linear decrease with T_1. And the 16 working fluid pairs can be divided into three parts, that could be attributed to the different thermophysical properties of the working fluids involved. Also, it is evident from the trend of m_{hp} that it is inconsistent with the trend of COP_{hp}, indicating that m_{hp} is not the primary influencing factor to COP_{hp} in this case. The increase in COP_{hp} is attributed to the rise in T_1, which results in an increase in stored heat and a decrease in work done by the compressor.

Figure 13 presents the effects of T_1 on the η_{ex}. In Figure 13, η_{ex} shows a linear increase with increasing T_1, and the trends of the 16 working fluid pairs are similar. It can be observed that at 65°C, the maximum value of η_{ex} is 51.89% of the working fluid pair R601a + R601a, and the minimum

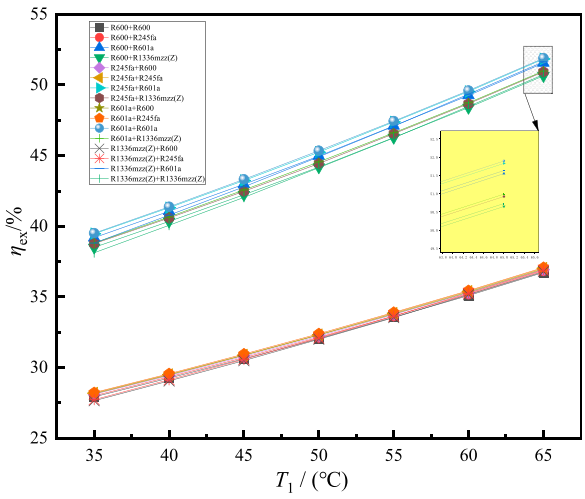

FIGURE 13
Effects of T_1 on the η_{ex}.

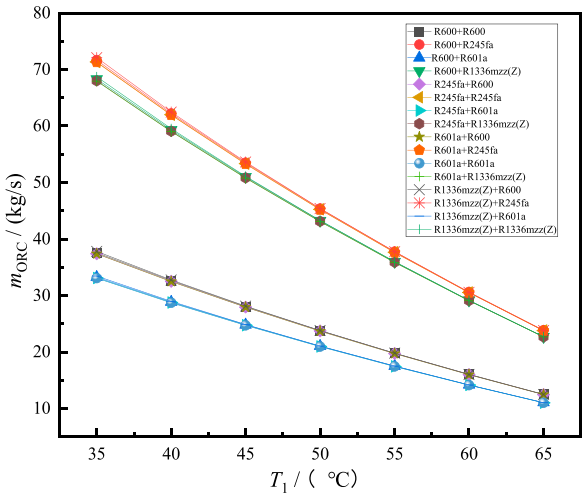

FIGURE 14
Effects of T_1 on the m_{COP}.

value of η_{ex} is 36.72% of the working fluid pair R600 + R600. This trend observed is roughly consistent with the η_{ptp} change and the improvement in the η_{ex} is primarily due to the increase in η_{ptp}.

Figure 14 reveals the effects of T_1 on the m_{ORC}. Referring to Figure 14, the 16 working fluid pairs can be divided into four parts, and m_{ORC} shows a linear decrease with increasing T_1. Therefore, although the flow rate changes in different subsystems may affect certain aspects, they are not the main factors that affect the ORC-TIPTES overall energy efficiency.

6.2 Single-objective optimization results

To sum up, based on the above analysis, two working fluid pairs of R245fa + R245fa and R601a + R601a are selected for further single-objective optimization analysis. This section discusses the single-objective optimization results of η_{ptp} and η_{ex} in the ORC-TIPTES, aiming to select optimal operating conditions to improve the system's overall performance. Three parameters, including T_1 ($T_{eva,hp}$), T_5 (T_{cs}), and T_6 (T_{ts}), are chosen as decision variables, and the corresponding ranges are shown in Table 5.

TABLE 5 Ranges of the decision variables.

Term	T_1/(°C)	T_5/(°C)	T_6/(°C)
R245fa + R245fa	[45,65]	[65,90]	[105,135]
R601a + R601a	[45,65]	[65,90]	[105,135]

TABLE 6 Results of the single-objective optimization with the objective function of η_{ptp}.

Term	T_1/(°C)	T_5/(°C)	T_6/(°C)	η_{ptp}/(%)
R245fa + R245fa	65	82.5	111	56.97
R601a + R601a	65	72.5	108	52.35

TABLE 7 Results of the single-objective optimization with the objective function of η_{ex}.

Term	T_1/(°C)	T_5/(°C)	T_6/(°C)	η_{ex}/(%)
R245fa + R245fa	65	82.5	111	33.57
R601a + R601a	65	72.5	108	30.11

Table 6 and Table 7 display the optimization results of R245fa + R245fa and R601a + R601a. It can be seen that the optimization values of η_{ptp} and η_{ex} for the working fluid pair R245fa + R245fa are greater than those of the working fluid pair R601a + R601a. However, both the values of η_{ptp} and η_{ex} of the working fluid pair R245fa + R245fa and R601a + R601a are very close. For working fluid pair R245fa + R245fa, η_{ptp} and η_{ex} are 56.97% and 33.57% when T_1, T_5, and T_6 are 65°C, 82.5°C and 111°C, respectively. Meanwhile, η_{ptp} of the working fluid pair R601a + R601a is 52.35%, and the values of η_{ex} is 30.11% when T_1, T_5, and T_6 are 65°C, 72.5°C, and 108°C. Therefore, it can be observed that the higher the evaporation temperature of the heat pump, the greater the system power efficiency and exergy efficiency. Additionally, when comparing the thermodynamic performance of these different working pairs of the ORC-TIPTES, it can be concluded that the performance of the working fluid pair of R245fa + R245fa is the best.

6.3 Analysis of single-objective optimization results

In this section, exergy destruction distributions are analyzed based on the optimization results. Figure 15 shows the exergy destruction and proportion of each component in the working

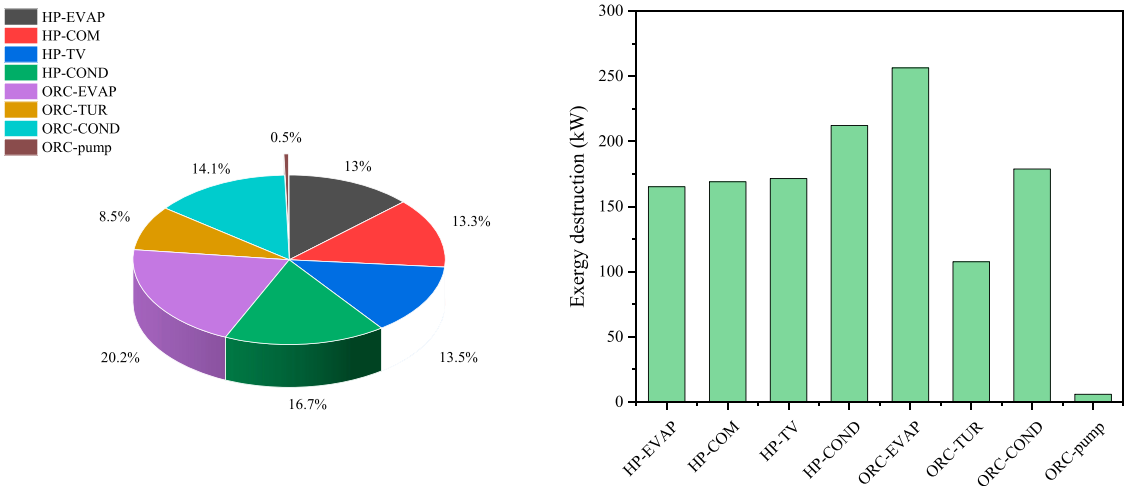

FIGURE 15
Exergy destruction and proportion of each component in working fluid pair of R245fa + R245fa.

fluid pair of R245fa + R245fa. The HP-EVAP, HP-COM, HP-TV, and HP-COND are components in the HP subsystem while ORC-EVAP, ORC-TUR, ORC-COND, and ORC-pump are respective components in the ORC subsystem. Among all components, the exergy destruction ratio of the ORC-EVAP is the largest at 20.2%, with a value of 256.31 kW. The proportion of exergy destruction in the HP-COND is relatively high, accounting for 16.7% and 212.11 kW while the exergy destruction in the ORC-COND is 178.73 kW accounting for 14.1% of the total exergy destruction. The exergy destructions of HP-EVAP, HP-COM, and HP-TV are 165.22 kW, 169.02 kW, and 171.43 kW, and their specific proportions are 13%, 13.3%, and 13.5%, respectively. The minimum exergy destruction is the ORC-pump of about 6.02 kW, accounting for only 0.5% of the total. For ORC-EVAP, the main reason for large exergy degradation is the large temperature difference during the heat transfer, which can be improved by appropriately reducing the temperature difference.

7 Conclusion

In this study, a system of ORC-TIPTES is built to test the effect of different combinations of working fluid pairs on the system performance. Further, the working fluid pairs of R245fa + R245fa and R601a + R601a are selected for single-objective optimization and the results based on the optimization were analyzed and discussed. The primary conclusions are as follows:

1) The effects of T_6 and T_1 on the system's η_{ptp} and η_{ex} are opposite. An increase in T_6 results in a decrease in both η_{ptp} and η_{ex}, while an increase in T_1 leads to an increase in both η_{ptp} and η_{ex}.
2) Based on the single-objective optimization results, the values of η_{ptp} and η_{ex} for the working fluid pair R245fa + R245fa surpass those of the R601a + R601a pair. The thermodynamic performance of the former system is superior to that of the latter one.
3) Conducting an exergy destruction analysis of the system based on the optimization results. Among all the system components, the evaporator in the ORC subsystem exhibits the highest exergy destruction, accounting for 20.2% of the total.

Data availability statement

The original contributions presented in the study are included in the article/Supplementary material, further inquiries can be directed to the corresponding author.

Author contributions

XJ: Writing–original draft. XZ: Software, Writing–original draft. RW: Validation, Writing–review and editing. XW: Conceptualization, Methodology, Writing–review and editing.

Funding

The author(s) declare financial support was received for the research, authorship, and/or publication of this article. This work is supported by the National Natural Science Foundation of China (Grant Number 52106006) and the science and technology project of Henan Province (Grant Number 222102320254).

Conflict of interest

Authors XJ, XZ, and RW were employed by PowerChina Chongqing Engineering Co., Ltd.

The remaining authors declare that the research was conducted in the absence of any commercial or financial relationships that could be construed as a potential conflict of interest.

Publisher's note

References

Agency, International Energy (2022). *Renewables 2022: analysis and forecast to 2027*. Available at https://www.iea.org/reports/renewables-2022.

Amirante, R., Cassone, E., Distaso, E., and Tamburrano, P. (2017). Overview on recent developments in energy storage: mechanical, electrochemical and hydrogen technologies. *Energy Convers. Manag.* 132, 372–387. doi:10.1016/j.enconman.2016.11.046

Bao, J., and Zhao, L. (2013). A review of working fluid and expander selections for organic Rankine cycle. *Renew. Sustain. Energy Rev.* 24, 325–342. doi:10.1016/j.rser.2013.03.040

Bellos, E., Tzivanidis, C., and Said, Z. (2021). Investigation and optimization of a solar-assisted pumped thermal energy storage system with flat plate collectors. *Energy Convers. Manag.* 237, 114137. doi:10.1016/j.enconman.2021.114137

Benato, A., and Stoppato, A. (2018). Pumped thermal electricity storage: a technology overview. *Therm. Sci. Eng. Prog.* 6, 301–315. doi:10.1016/j.tsep.2018.01.017

Blanquiceth, J., Cardemil, J., Henríquez, M., and Escobar, R. (2023). Thermodynamic evaluation of a pumped thermal electricity storage system integrated with large-scale thermal power plants. *Renew. Sustain. Energy Rev.* 175, 113134. doi:10.1016/j.rser.2022.113134

Blondel, Q., Tauveron, N., Lhermet, G., and Caney, N. (2023). Zeotropic mixtures study in plate heat exchangers and ORC systems. *Appl. Therm. Eng.* 219, 119418. doi:10.1016/j.applthermaleng.2022.119418

Deguenon, L., Yamegueu, D., Moussa Kadri, S., and Gomna, A. (2023). Overcoming the challenges of integrating variable renewable energy to the grid: a comprehensive review of electrochemical battery storage systems. *J. Power Sources* 580, 233343. doi:10.1016/j.jpowsour.2023.233343

Eppinger, B., Steger, D., Regensburger, C., Karl, J., Schlücker, E., and Will, S. (2021). Carnot battery: simulation and design of a reversible heat pump-organic Rankine cycle pilot plant. *Appl. Energy* 288, 116650. doi:10.1016/j.apenergy.2021.116650

Eppinger, B., Zigan, L., Karl, J., and Will, S. (2020). Pumped thermal energy storage with heat pump-ORC-systems: comparison of latent and sensible thermal storages for various fluids. *Appl. Energy* 280, 115940. doi:10.1016/j.apenergy.2020.115940

Fan, R., and Xi, H. (2022a). Exergoeconomic optimization and working fluid comparison of low-temperature Carnot battery systems for energy storage. *J. Energy Storage* 51. doi:10.1016/j.est.2022.104453

Fan, R., and Xi, H. (2022b). Energy, exergy, economic (3E) analysis, optimization and comparison of different Carnot battery systems for energy storage. *Energy Convers. Manag.* 252, 115037. doi:10.1016/j.enconman.2021.115037

Frate, G., Antonelli, M., and Desideri, U. (2017). A novel Pumped Thermal Electricity Storage (PTES) system with thermal integration. *Appl. Therm. Eng.* 121, 1051–1058. doi:10.1016/j.applthermaleng.2017.04.127

Frate, G., Ferrari, L., and Desideri, U. (2021). Energy storage for grid-scale applications: technology review and economic feasibility analysis. *Renew. Energy* 163, 1754–1772. doi:10.1016/j.renene.2020.10.070

Fu, H., He, Q., Song, J., and Hao, Y. (2021). Thermodynamic of a novel solar heat storage compressed carbon dioxide energy storage system. *Energy Convers. Manag.* 247, 114757. doi:10.1016/j.enconman.2021.114757

Hu, S., Yang, Z., Li, J., and Duan, Y. (2021). Thermo-economic analysis of the pumped thermal energy storage with thermal integration in different application scenarios. *Energy Convers. Manag.* 236, 114072. doi:10.1016/j.enconman.2021.114072

Jockenhöfer, H., Steinmann, W., and Bauer, D. (2018). Detailed numerical investigation of a pumped thermal energy storage with low temperature heat integration. *Energy* 145, 665–676. doi:10.1016/j.energy.2017.12.087

Li, X., Xu, B., Tian, H., and Shu, G. (2021). Towards a novel holistic design of organic Rankine cycle (ORC) systems operating under heat source fluctuations and intermittency. *Renew. Sustain. Energy Rev.* 147, 111207. doi:10.1016/j.rser.2021.111207

Liang, T., Vecchi, A., Knobloch, K., Sciacovelli, A., Engelbrecht, K., Li, Y., et al. (2022). Key components for Carnot Battery: technology review, technical barriers and selection criteria. *Renew. Sustain. Energy Rev.* 163, 112478. doi:10.1016/j.rser.2022.112478

Lin, B., and Zhang, Q. (2023). The transfer of energy-intensive projects under carbon constraints: does energy structure matter? *Energy* 284, 128661. doi:10.1016/j.energy.2023.128661

Liu, L., Zhang, S., Jiao, Y., Liu, X., Li, G., Liu, C., et al. (2023b). Thermodynamic and heat transfer performance of the organic triangle cycle. *Process. (Basel)* 11, 357. doi:10.3390/pr11020357

Liu, Z., Li, M., Virguez, E., and Xie, X. (2023a). Low-carbon transition pathways of power systems for Guangdong-Hongkong-Macau Region in China. *Energy Environ. Sci.* doi:10.1039/d3ee02181e

Luo, X., Wang, J., Dooner, M., and Clarke, J. (2015). Overview of current development in electrical energy storage technologies and the application potential in power system operation. *Appl. Energy* 137, 511–536. doi:10.1016/j.apenergy.2014.09.081

Ökten, K., and Kurşun, B. (2022). Thermo-economic assessment of a thermally integrated pumped thermal energy storage (TI-PTES) system combined with an absorption refrigeration cycle driven by low-grade heat source. *J. Energy Storage* 51, 104486. doi:10.1016/j.est.2022.104486

Olabi, A., Onumaegbu, C., Wilberforce, T., Ramadan, M., Abdelkareem, M., and Al Alami, A. (2021). Critical review of energy storage systems. *Energy* 214, 118987. doi:10.1016/j.energy.2020.118987

Peterson, R. B. (2011). A concept for storing utility-scale electrical energy in the form of latent heat. *Energy* 36, 6098–6109. doi:10.1016/j.energy.2011.08.003

Sun, Z., Liu, C., Xu, X., Li, Q. B., Wang, X., Wang, S., et al. (2019). Comparative carbon and water footprint analysis and optimization of Organic Rankine Cycle. *Appl. Therm. Eng.*, 158.

Tafone, AAPR, Pili, R., Pihl Andersen, M., and Romagnoli, A. (2023). Dynamic modelling of a compressed heat energy storage (CHEST) system integrated with a cascaded phase change materials thermal energy storage. *Appl. Therm. Eng.* 226, 120256. doi:10.1016/j.applthermaleng.2023.120256

Tang, J., Li, Q., Wang, S., and Yu, H. (2023). Thermo-economic optimization and comparative analysis of different organic flash cycles for the supercritical CO_2 recompression Brayton cycle waste heat recovery. *Energy* 278, 128002. doi:10.1016/j.energy.2023.128002

Tang, J., Zhang, Q., Zhang, Z., Li, Q., Wu, C., and Wang, X. (2022). Development and performance assessment of a novel combined power system integrating a supercritical carbon dioxide Brayton cycle with an absorption heat transformer. *Energy Convers. Manag.* 251, 114992. doi:10.1016/j.enconman.2021.114992

Tillmanns, DAPD, Pell, D., Schilling, J., and Bardow, A. (2022). The thermo-economic potential of ORC-based pumped-thermal electricity storage: insights from the integrated design of processes and working fluids. *Energy Technol.* 10. doi:10.1002/ente.202200182

Wang, P., Li, Q., Liu, C., Wang, R., Luo, Z., Zou, P., et al. (2022a). Comparative analysis of system performance of thermally integrated pumped thermal energy storage systems based on organic flash cycle and organic Rankine cycle. *Energy Convers. Manag.* 273, 116416. doi:10.1016/j.enconman.2022.116416

Wang, P., Li, Q., Wang, S., He, C., and Tang, J. (2023b). Thermo-economic analysis and comparative study of different thermally integrated pumped thermal electricity storage systems. *Renew. Energy* 217, 119150. doi:10.1016/j.renene.2023.119150

Wang, Q., Macián-Juan, R., and Li, D. (2022c). Analysis and assessment of a novel organic flash Rankine cycle (OFRC) system for low-temperature heat recovery. *Energy Sci. Eng.* 10, 3023–3043. doi:10.1002/ese3.1186

Wang, S., Liu, C., Li, Q., Liu, L., Huo, E., and Zhang, C. (2020). Selection principle of working fluid for organic Rankine cycle based on environmental benefits and economic performance. *Appl. Therm. Eng.* 178, 115598. doi:10.1016/j.applthermaleng.2020.115598

Wang, S., Liu, C., Ren, J., Liu, L., Li, Q., and Huo, E. (2019). Carbon footprint analysis of organic Rankine cycle system using zeotropic mixtures considering leak of fluid. *J. Clean. Prod.* 239, 118095. doi:10.1016/j.jclepro.2019.118095

Wang, S., Liu, C., Tang, J., Xiao, T., Huo, E., and Guan, Z. (2023a). Multi-mode and exergoeconomic analysis of a novel combined cooling, heating, and power system applied in the geothermal field. *Energy Convers. Manag.* 276, 116565. doi:10.1016/j.enconman.2022.116565

Wang, S., Liu, C., Zhang, S., Li, Q., and Huo, E. (2022b). Multi-objective optimization and fluid selection of organic Rankine cycle (ORC) system based on economic-environmental-sustainable analysis. *Energy Convers. Manag.* 254, 115238. doi:10.1016/j.enconman.2022.115238

Wang, S., Zhang, L., Liu, C., Liu, Z., Lan, S., Li, Q. B., et al. (2021). Techno-economic-environmental evaluation of a combined cooling heating and power system for gas turbine waste heat recovery. *Energy* 231, 120956. doi:10.1016/j.energy.2021.120956

Wang, X., and Dai, Y. (2016). Exergoeconomic analysis of utilizing the transcritical CO2 cycle and the ORC for a recompression supercritical CO2 cycle waste heat recovery: a comparative study. *Appl. Energy* 170, 193–207. doi:10.1016/j.apenergy.2016.02.112

Xue, X., Zhao, Y., and Zhao, C. (2022). Multi-criteria thermodynamic analysis of pumped-thermal electricity storage with thermal integration and application in electric peak shaving of coal-fired power plant. *Energy Convers. Manag.* 258, 115502. doi:10.1016/j.enconman.2022.115502

Yu, W., Li, Q., Liu, C., Liu, L., and Xu, X. (2023). Decomposition mechanism of hydrofluorocarbon (HFC-245fa) in supercritical water: a ReaxFF-MD and DFT study. *Int. J. Hydrogen Energy* 48, 864–878. doi:10.1016/j.ijhydene.2022.10.013

Zhang, S., Li, Y., Du, E., Fan, C., Wu, Z., Yao, Y., et al. (2023). A review and outlook on cloud energy storage: an aggregated and shared utilizing method of energy storage system. *Renew. Sustain. Energy Rev.* 185, 113606. doi:10.1016/j.rser.2023.113606

Zhang, Y., and Xie, Z. (2022). Thermodynamic efficiency and bounds of pumped thermal electricity storage under whole process ecological optimization. *Renew. Energy* 188, 711–720. doi:10.1016/j.renene.2022.02.073

Zhao, Y., Song, J., Liu, M., Zhang, K., Markides, C. N., and Yan, J. (2023). Multi-objective thermo-economic optimisation of Joule-Brayton pumped thermal electricity storage systems: role of working fluids and sensible heat storage materials. *Appl. Therm. Eng.* 223, 119972. doi:10.1016/j.applthermaleng.2023.119972

Nomenclature

Symbols

COP	coefficient of performance
h	specific enthalpy (kJ/kg)
P	pressure (kPa)
m	mass flow rate (kg/s)
T	temperature (°C)
Q	heat (kW)
W	power (kW)

Abbreviations

ARC	Absorption refrigeration cycle
CHEST	Compressed heat energy storage
PHS	Humped hydro energy storage
PTES	Pumped thermal energy storage
TI-PTES	Thermally integrated PTES
OFC	Organic flash cycle
ORC	Organic Rankine cycle
GWP	Global Warming Potential
ODP	Ozone Depletion Potential
HP	Heat Pump
TES	Thermal Energy Storage System

Greek letters

η	efficiency
τ	storage duration (h)
ρ	density (kg/m^3)

Subscripts/superscripts

he	heat exchanger
tur	turbine
eva	evaporator
com	compressor
pum	pump
ptp	power-to-power
out	outlet
in	inlet
w	working fluid
0	environment
np	net power
pp	pinch point
hp	heat pump
dt	discharging part
st	storage tank
con	condenser
ts	TES subsystem
hs	heat source
cs	cold storage